Punjab University Journal of Mathematics (2024), 56(6), 315-333
https://doi.org/10.52280/pujm.2024.56(6)05

Stratified Hydromagnetic Gas-Liquid Flow in a Wavy Channel

Ghulam Fatima[1], Ambreen Afsar Khan[1*]
Department of Mathematics and Statistics,
International Islamic University, Islamabad, Pakistan,
Email: ambreen.afsar@iiu.edu.pk

Received: 14 Novemberl, 2024 / Accepted: 10 January, 2025 / Published online: 31 January, 2025

Abstract. This research theoretically explores the behavior of a two-phase flow within a channel, particularly focusing on the interaction between stratified gas and liquid flow when a magnetic field is present. The study excludes consideration of mixing between the phases. The governing equations for this two-phase flow system contain momentum equation, continuity equation for both phases (accounting for compressibility effects in the gas phase), and magnetic effects. Peristaltic motion is simulated using appropriate boundary conditions reflecting the rhythmic contractions and expansions of the channel walls, influencing the flow dynamics of the two phases. To analyze how key parameters such as flow rates, channel geometry, and magnetic field strength affect flow characteristics, a perturbation approach is employed. The study examines the formation of wave patterns and variations in flow velocities resulting from the complex interactions between phases and the magnetic field, presenting graphical data to illustrate these phenomena. The Reynolds number and magnetic parameter are observed to slow down the flow rate as well as velocity of both regions. The compressibility parameter and Knudsen number decreases the velocity of fluid flow in both regions. By increasing the viscosity ratio, the velocity of the fluid slowdowns. The findings will contribute to understand the complex interplay between peristaltic motion and hydromagnetic forces in two-phase flows, with potential implications for diverse fields such as industrial processes and biomedical engineering.

AMS (MOS) Subject Classification Codes: 76T10; 76Wxx; 35A24
Key Words: Wavy Channel, gas-liquid two-phase flow, Hydromagnetic flow, Perturbation Technique.

1. Introduction

Peristalsis, the rhythmic contraction and relaxation of muscles in tubular structures like the digestive tract or blood vessels, has inspired various innovations. These include waste

passage control pumps, heart-lung machines, and pharmaceutical medication delivery systems, all of which make use of this natural occurrence to operate efficiently [14]. In light of the aforementioned uses, multiple mathematical representations of the peristaltic process have been incorporated into the published works. It can be used in equipment like sanitary transport in addition to biomedical ones. Engelmann [8] conducted research on the existence of waves of peristaltic in the ureters. It was Latham who initially explored the mechanism of the flow of fluid using a peristaltic pump [16]. Building on the seminal work of Latham, Shapiro [29] explored peristalsis under assumptions of creeping flow and advanced the mathematical modeling of peristaltic transport. Recently, Rashid et al. [27] studied Williamson fluid peristaltic flow with an induced magnetic field in a curved channel. Convective conditions and wall characteristics in MHD radiative peristalsis flow of Eyring–Powell nanofluid flow was examined by Nisar et al. [19]. Additionally, the nature of the fluid, wall characteristics, conduit geometry, variations in viscosity, and other relevant processes are among the significant factors taken into account in a number of mathematical representations of the peristaltic mechanism, which have been examined lately by [1, 17, 22, 32].

There is currently a noticeable trend for researchers to become more interested in the transport of compressible flow. Many technological and natural processes use knowledge of compressed air flow. Compressible fluid flow refers to the movement of a fluid in which changes in pressure and temperature significantly affect its density. For scientists and engineers working in situations with high fluid velocities or where temperature and pressure change quickly, an understanding of compressible flow is essential. In order to examine a decreased stream rate for slip and non-slip fluid, Mekheimer et al. [18] evaluated the impact of MHD on Maxwell compressible fluid generated by a wave propagating in a porous microchannel. Some novel researches on compressible fluid flow in various geometries was conducted by Canuto and Taira [5], Wu et al. [34], and Jarauta et al. [12]. Eldesoky et al. [7] examined the Peristaltic flow of a compressible Maxwellian fluid via an axisymmetric cylindrical conduit. In the subject of compressible flow, Rafaqat and Khan [20] have recently made significant contributions by examining the impact of porosity in an asymmetric channel. In the same context, numerical approach was used to solve compressible flow phenomenon by Rafaqat and Khan [21].

When two different phases move simultaneously within a system, usually a liquid phase and a gas phase, this is referred to as two-phase flow. This type of flow is prevalent in numerous industrial and natural processes, including oil and gas transportation, chemical reactors, nuclear power plants, and environmental systems. Shukla et al. [30] used the two-fluid model to simulate peristaltic flow via axisymmetric and channel geometries. The investigation of Shukla et al. [30] for an irregular axisymmetric tube was expanded by Srivastava and Saxena [31]. Afterwards, a number of scholars examined other fluid models and geometries in order to expand on this concept. Rao and Usha [26] thoroughly described the characteristics of confined boluses and examined the peristaltic flow of two-fluid phenomenon in the tube. Herschel-Bulkley Model for peristaltic transfer of two-layered blood flow was studied by Rajashekhar et al. [23]. Ranjit et al. [25] examined the peristaltically generated microchannel's two-layered electroosmotic flow: entropy formation and Joule heating. Zhang et al. [35] numerically investigated gas-liquid two-phase flow through a plate orifice equipped horizontal pipe. Electrothermal study in peristaltic pumping in an

asymmetric microchannel to two-layered couple stress fluid flow was carried by Ranjit et al. [24]. A new deep learning technique based on complicated networks for describing gas-liquid two-phase flow was developed by Gao et al. [9]. Chemically reactive flow of immiscible viscous Casson fluids in a revolving conduit was explored by Alzahrani et al. [4]. The assessment of gas/liquid flow rates using thermal diffusion and the distribution law of Taylor bubble/liquid slug length in oil-gas-water slug flow was investigated by Guo et al. [10]. Wang et al. [33] studied the change of the gas-oil two-phase flow pattern in a huge vertical annulus by experimentation. Numerical modeling for the analysis of air-water two-phase flow dynamics in complex U-bend systems was investigated by Kükrer and Eskin [15]. In gas–liquid slug flow in capillaries, a Navier-slip model for liquid film thickness was investigated by Hussain and Gupta [11].

Magnetohydrodynamics (MHD) in conjunction with sinusoidal waves is very important, especially in the treatment of cancerous tumors, the use of magnetic resonance imaging (MRI) to diagnose infections and vascular and brain disorders, blood pressure regulation, and magnetotherapy [23, 26]. An electric current is created when a conducting fluid passes through a magnetic field. The fluid's flow dynamics can be changed by the Lorentz force, which is created when this current interacts with the magnetic field. Ali et al. [3] investigates the bioconvective slip flow of a radiating magneto-cross-nanomaterial over a stretching cylinder with activation energy. Magneto-copper-titania/water-ethylene glycol stream dynamics within a gyrating channel was studied by Das et al. [6]. The peristaltic transportation of Jeffrey hybrid nano-blood model via an artery with a resonant magnetic field was discussed by Ali et al. [2].

A detailed analysis of the literature discloses that the simultaneous consideration of two-phase flow dynamics and peristaltic motion presents a multifaceted interaction that has not been explored. In present article, stratified gas-liquid flow is considered with no mixing between the phases. The presence of a magnetic field influences the dynamics of the gas and liquid, and peristalsis induces rhythmic contractions and expansions within the channel. The governing equations of each phase are incorporated with the addition of MHD effect. Perturbation method is applied to find analytic solution of the problem. Graphical depiction of each phase for input variables is presented.

2. NOTATIONS AND PRELIMINARIES

Notation	**Description**
a_1^* , a_2^*	Amplitudes (m)
u, v	Axial and transverse velocity(ms^{-1})
χ	Compressibility parameter
ρ	Density at $p_c(kgm^{-3})$
σ	Electric Conductivity$(kg^{-1}m^{-3}s^3A^2)$
Q	Flow rate(m^3s^{-1})
(H_1, H_2)	Height of channel's walls (m)
B_0	Magnetic field intensity $(kgs^{-2}A^{-1})$
M	Magnetic parameter
ϕ	Phase difference
p	Pressure(Nm^{-2})
p_c	Reference Pressure(Nm^{-2})
Ra	Reynold number
λ	Sinusoidal wavelength (m)
k_n	Slip Parameter
x, y	Spatial Coordinates(m)
c	Speed of wave(ms^{-1})
$i = I, II$	Subscript used for liquid and gas region
μ	Viscosity ratio
A	Wave number

3. PROBLEM FORMULATION

Consider stratified two phase peristaltic flow in a channel of width d_1+d_2. Stratified regime features distinct layers of gas and liquid phases flowing parallel to each other, with minimal mixing between the layers. The channel's walls (H_1, H_2) are placed at (d_1, d_2) from the geometry's centerline, correspondingly. A sinusoidal wave λ causes the peristaltic flow that produce waves with varying amplitudes a_1^* and a_2^* and phase difference ϕ $(0 \leq \phi \leq \pi)$ and propagates with speed c along the channel walls. In the transversal direction, a magnetic field with intensity B_0 is applied. The wall surfaces' geometric configuration is [21]

$$H_1(x,t) = d_1 + a_1^* \cos\left(\frac{2\pi}{\lambda}(x - ct)\right),$$

$$H_2(x,t) = -d_2 - a_2^* \cos\left(\frac{2\pi}{\lambda}(x - ct) + \phi\right). \tag{3. 1}$$

Region I

Region I takes liquid into account. Water will be stated in superscript I throughout this paper.

$$v_y + u_x = 0, \tag{3. 2}$$

$$\rho(uu_x + u_t + vu_y) = -p_x - \sigma {B_0}^2 u + \mu \nabla^2 u, \tag{3. 3}$$

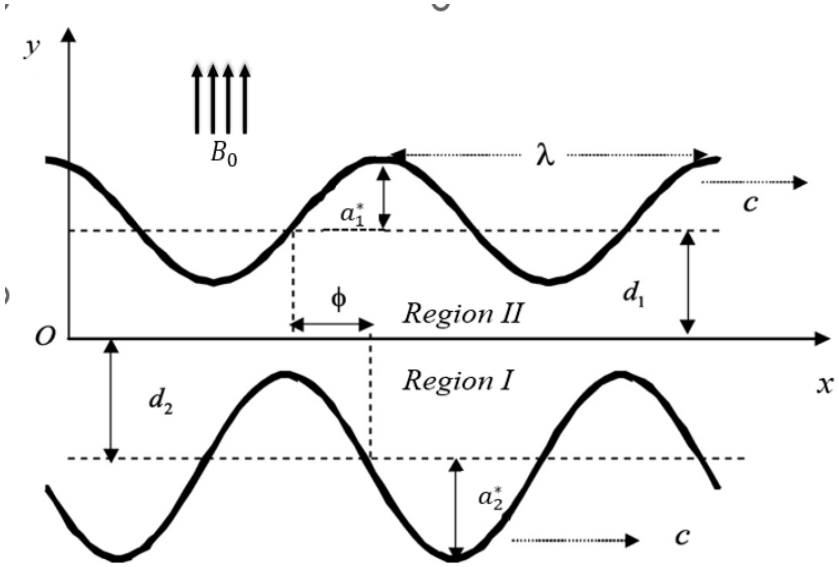

FIGURE 1. Geometry of the flow

$$\rho\left(vv_y + v_t + uv_x\right) = +\mu\nabla^2 v - p_y, \tag{3. 4}$$

Region II

The upper section, known as region II, where gas is taken into account. The superscript II will be used throughout the article to refer to air. The governing equations are defined as [21]

$$\rho_t + u\rho_x + \left(u_x + v_y\right)\rho = -v\rho_y, \tag{3. 5}$$

$$\rho\left(vu_y + u_t + uu_x\right) = -\sigma {B_0}^2 u - p_x + \mu\left[\frac{1}{3}\frac{\partial}{\partial x}\left(u_x + v_y\right) + \nabla^2 u\right], \tag{3. 6}$$

$$\rho\left(uv_x + v_t + vv_y\right) = +\mu\left[\frac{1}{3}\frac{\partial}{\partial y}\left(u_x + v_y\right) + \nabla^2 v\right] - p_y. \tag{3. 7}$$

The following is a description of pressure-based density:

$$\rho_p = \rho k_f,$$

which has solution as

$$\rho = \rho_0 exp\left(k_f\left(p - p_c\right)\right), \tag{3. 8}$$

The slip boundary condition is considered at the channel walls. It is considered that stresses and velocity will continue at the interface. [21, 24, 25]

$$Aty = 0, \qquad v^{II} = v^I, \qquad u^{II} = u^I, \quad \tau_{xy}^I = \tau_{xy}^{II}, \quad p^I = \ p^{II},$$

$$Aty = H_1, \qquad u^{II} = -Su_y^{II}\ , \quad v^{II} = \frac{\partial \eta_1}{\partial t}$$

$$Aty = H_2, \qquad v^I = -\frac{\partial \eta_2}{\partial t}, \qquad u^I = Su_y^I. \tag{3. 9}$$

Here, the vertical displacement from mean position d_1 and d_2 are identified by η_1 and η_2, respectively.
The subsequent parameters and non-dimensional variables are designated as

$$x^{i*} = \frac{x^i}{d_i},\ y^{i*} = \frac{y^i}{d_i},\ \rho^* = \frac{\rho}{\rho_0}, u^{i*} = \frac{u^i}{c}, v^{i*} = \frac{v^i}{c},\ t^* = \frac{ct}{d},\ p^* = \frac{p}{\rho_0 c^2},\ h_1 = \frac{H_1}{d_1},$$

$$p_c{}^* = \frac{p_c}{\rho_0 c^2},\ h_2 = \frac{H_2}{d_1}\ \alpha = \frac{2\pi d_i}{\lambda},\ Ra = \frac{\rho_0 cd}{\mu_i},\ \chi = \rho_0 k_c c^2. \tag{3. 10}$$

Here, $i = I,\ II$ region. The following is the expression for the dimensionless version of equations (5-8) and (2-4):

Region I

$$u_x = -v_y, \tag{3. 11}$$

$$(uu_x + u_t + vu_y) = -p_x - Mu + \frac{1}{Ra}\nabla^2 u, \tag{3. 12}$$

$$(uv_x + v_t + vv_y) = -p_y + \frac{1}{Ra}\nabla^2 v. \tag{3. 13}$$

Region II

$$\rho - exp\left(\chi\left(p - p_c\right)\right) = 0, \tag{3. 14}$$

$$\rho_t + u\rho_x + \left(u_x + v_y\right)\rho = -v\rho_y, \tag{3. 15}$$

$$\rho\left(vu_y + u_t + uu_x\right) = -Mu - p_x + \left[\frac{1}{3}\frac{\partial}{\partial x}\left(u_x + v_y\right) + \nabla^2 u\right]\frac{1}{Ra}, \tag{3. 16}$$

$$\rho\left(vv_y + v_t + uv_x\right) = +\frac{1}{Ra}\left[\nabla^2 v + \frac{1}{3}\frac{\partial}{\partial y}\left(u_x + v_y\right)\right] - p_y, \tag{3. 17}$$

$$h_1 = 1 + \eta_1\left(x,t\right), \quad h_2 = -d^* - \eta_2\left(x,t\right),$$

here $\eta_1 = \epsilon cos\left(\alpha\left(x-t\right)\right), \quad \eta_2 = a\epsilon cos\left(\alpha\left(x-t\right)+\phi\right), \quad d^* = \frac{d_2}{d_1}, \quad a = \frac{a_2}{a_1}.$

4. Solution Methodology

We consider $u_i = u_{0i}\left(y\right),$ and $v = 0$ with $\frac{dp_i}{dx} = Constant = \frac{dp_{0_i}}{dx}$, for steady parallel flow. The system (3. 11)–(3. 17) will have a solution in the form

$$u_{0_I}(y) = \frac{Ra}{\xi^2}\frac{\begin{array}{c} -\left(\begin{array}{c}\mu\left(1+k_n\xi+e^{2\xi}\left(-1+k_n\xi\right)\right)\left(-1-k_n\xi+{}^{2d^*\xi}\left(-1+k_n\xi\right)\right)\\ +d^*\left(-1-k_n\xi+{}^{2\xi}\left(-1+k_n\xi\right)\right)\left(1+k_n\xi+{}^{2d^*\xi}\left(-1+k_n\xi\right)\right)\end{array}\right)\frac{dp_{0_1}}{dx}+\\ {}^{(d+y)\xi}\left(\begin{array}{c}\left(\begin{array}{c}-\mu\left(1+k_n\xi+{}^{2\xi}\left(-1+k_n\xi\right)\right)+d^*\left(-1-k_n\xi+{}^{2\xi}\left(-1+k_n\xi\right)\right)\\ \left(1+{}^{d^*\xi}\left(-1+k_n\xi\right)\right)\end{array}\right)\frac{dp_{0_1}}{dx}\\ -d^{*d^*\xi}\left(-1+k_n\xi\right)\left(-1+k_n\xi\right)\left(1+k_n\xi+{}^{\xi}\left(-1+k_n\xi\right)\right)\frac{dp_{0_2}}{dx}\end{array}\right)-\\ -{}^{y\xi}\left(\begin{array}{c}\left(\begin{array}{c}d^*\left(-1+{}^{d^*\xi}-k_n\xi\right)\left(-1-k_n\xi+{}^{2\xi}\left(-1+k_n\xi\right)\right)+\\ {}^{d^*\xi}\mu\left(1+k_n\xi+{}^{2\xi}\left(-1+k_n\xi\right)\right)\end{array}\right)\frac{dp_{0_1}}{dx}+\\ d^*\left(-1+k_n\xi\right)\left(1+k_n\xi\right)\left(1+k_n\xi+{}^{\xi}\left(-1+k_n\xi\right)\right)\frac{dp_{0_2}}{dx}\end{array}\right)\end{array}}{\begin{array}{c}\mu\left(1+k_n\xi+{}^{2\xi}\left(-1+k_n\xi\right)\right)\left(-1-k_n\xi+{}^{2d^*\xi}\left(-1+k_n\xi\right)\right)+d^*\left(-1-k_n\xi+{}^{2\xi}\left(-1+k_n\xi\right)\right)\\ \left(1+k_n\xi+{}^{2d^*\xi}\left(-1+k_n\xi\right)\right)\end{array}},$$

$$u_{0_{II}}(y) = -\frac{Ra}{\xi^2}\frac{\begin{pmatrix} -y\xi\left(\mu\left(-1+{}^{d^*\xi}\right)\left(1+k_n\xi+{}^{d^*\xi}\left(-1+k_n\xi\right)\right)\left({}^{2\xi}\left(-1+k_n\xi\right)+{}^{2y\xi}\left(1+k_n\xi\right)\right)\frac{dp_{0_1}}{dx}\right)+ \\ \left(\begin{array}{c} d^*\left(1+k_n\xi+{}^{2d^*\xi}\left(-1+k_n\xi\right)\right)\left(\xi+{}^{\xi+2y\xi}+{}^{(2+y)\xi}\left(1+k_n\xi\right)-{}^{y\xi}\left(1+k_n\xi\right)\right)+ \\ \mu\left({}^{\xi(1+2d^*)}\left(1-k_n\xi\right)+{}^{\xi(1+2d^*+2y)}\left(-1+k_n\xi\right)\right)-{}^{2(1+d^*)\xi}\left(-1+k_n\xi\right)^2+ \\ {}^{(2+2d^*+y)\xi}\left(-1+k_n\xi\right)^2+{}^{\xi}\left(1+k_n\xi\right)-{}^{\xi(1+2y)}\left(1+k_n\xi\right) \\ -{}^{y\xi}\left(1+k_n\xi\right)^2+{}^{2y\xi}\left(1+k_n\xi\right)^2+\left({}^{(2+y)\xi}+{}^{2(d^*+y)\xi}\right) \\ \left(1-{k_n}^2\xi^2\right)+\left({}^{(2d^*+y)\xi}+{}^{2\xi}\right)\left(-1+{k_n}^2\xi^2\right)\frac{dp_{0_2}}{dx} \end{array}\right) \end{pmatrix}}{\begin{array}{c}\mu\left(1+k_n\xi+{}^{2\xi}\left(-1+k_n\xi\right)\right)\left(-1-k_n\xi+{}^{2d^*\xi}\left(-1+k_n\xi\right)\right)+d^*\left(-1-k_n\xi+{}^{2\xi}\left(-1+k_n\xi\right)\right) \\ \left(1+k_n\xi+{}^{2d^*\xi}\left(-1+k_n\xi\right)\right)\end{array}}. \tag{4. 18}$$

To tackle the aforementioned problem, we use the regular perturbation method. As described by [4.19–4.22], we assume the pressure, density, and velocity components as follows:

$$p(x,y,t) = \epsilon p_1 + \epsilon^2 p_2 + ..., \tag{4. 19}$$

$$u(x,y,t) = \epsilon u_1 + \epsilon^2 u_2 + ..., \tag{4. 20}$$

$$v(x,y,t) = \epsilon v_1 + \epsilon^2 v_2 + \ldots, \tag{4. 21}$$

$$\rho(x,y,t) - 1 = \epsilon\rho_1 + \epsilon^2\rho_2 + \ldots. \tag{4. 22}$$

Through including Eqs. (4.19-4.21) to Eqs. (3.11-3.13) and Eqs. (4.19-4.22) to Eqs. (3.14-3.17).

For $O(\epsilon)$

Region I

$$\begin{gathered} v_{1y} = -u_{1x}, \\ u_{1t} - Mu_1 = +\frac{1}{Ra}\nabla^2 u_1 - p_{1x}, \\ v_{1t} + p_{1y} = +\frac{1}{Ra}\nabla^2 v_1, \end{gathered} \tag{4. 23}$$

Region II

$$\begin{gathered} \rho_1 - \chi p_1 = 0, v_{1y} + \rho_{1t} + u_{1x} = 0, \\ u_{1t} + p_{1x} = -Mu_1 + \frac{1}{Ra}\left[\nabla^2 u_1 + \frac{1}{3}\frac{\partial}{\partial x}\left(u_{1x} + v_{1y}\right)\right], \\ v_{1t} = -p_{1y} + \frac{1}{Ra}\left[\nabla^2 v_1 + \frac{1}{3}\frac{\partial}{\partial y}\left(u_{1x} + v_{1y}\right)\right]. \end{gathered} \tag{4. 24}$$

For $O(\epsilon^2)$

Region I

$$\begin{gathered} u_{2x} = -v_{2y}, \\ \left(u_1 u_{1x} + u_{2t} + v_1 u_{1y}\right) - p_{2x} = +\frac{1}{Ra}\nabla^2 u_2 - Mu_2, \\ \left(u_1 v_{1x} + v_{2t} + v_1 v_{1y}\right) - p_{2y} = +\frac{1}{Ra}\nabla^2 v_2, \end{gathered} \tag{4. 25}$$

Region II

$$\begin{gathered} \rho_2 = \chi p_2 + \frac{1}{2}(\chi p_1)^2, \\ \rho_{2t} + u_1\rho_{1x} + v_1\rho_{1y} + u_{2x} + v_{2y} + \rho_1\left(u_{1x} + v_{1y}\right) = 0, \end{gathered}$$

$$(u_{2t}+u_1u_{1x}+v_1u_{1y}+\rho_1u_{1t})=-p_{2x}+\frac{1}{Ra}\left[\nabla^2u_2+\frac{1}{3}\frac{\partial}{\partial x}(u_{2x}+v_{2y})\right]-Mu_2,$$

$$(v_{2t}+u_1v_{1x}+v_1v_{1y}+\rho_1v_{1t})=-p_{2y}+\frac{1}{Ra}\left[\nabla^2v_2+\frac{1}{3}\frac{\partial}{\partial y}(u_{2x}+v_{2y})\right], \quad (4.\ 26)$$

Since the waves are sinusoidal so we assume the solution in terms of harmonic wave solution.

$$p_1-\ e^{\iota\alpha(x-t)}P_1(y)=\overline{P_1}(y)\,e^{-\iota\alpha(x-t)}, \quad (4.\ 27)$$

$$u_1\ =e^{\iota\alpha(x-t)}\,U_1(y)+\ e^{-\iota\alpha(x-t)}\overline{U_1}(y), \quad (4.\ 28)$$

$$v_1\ =e^{\iota\alpha(x-t)}\,V_1(y)+e^{-\iota\alpha(x-t)}\overline{V_1}(y)\,, \quad (4.\ 29)$$

$$\rho_1\ =e^{\iota\alpha(x-t)}P_1(y)\ +\overline{P_1}(y)\,e^{-\iota\alpha(x-t)}, \quad (4.\ 30)$$

and

$$p_2=\ P_2(y)\,e^{2i\alpha(x-t)}\ +P_{20}(y)+e^{-2i\alpha(x-t)}\overline{P_2}(y)\,, \quad (4.\ 31)$$

$$u_2=\ U_2(y)\,e^{2i\alpha(x-t)}+U_{20}(y)\ +\overline{U_2}(y)\,e^{-2i\alpha(x-t)}, \quad (4.\ 32)$$

$$v_2=\ V_2(y)\,e^{2i\alpha(x-t)}+V_{20}(y)\ +\overline{V_2}(y)\,e^{-2i\alpha(x-t)}, \quad (4.\ 33)$$

$$\rho_2=\ D_2(y)\,e^{2i\alpha(x-t)}+D_{20}(y)\ +\overline{D_2}(y)\,e^{-2i\alpha(x-t)}. \quad (4.\ 34)$$

Region I

By adding Eqs. (27–29) to equation (4. 23), we get the subsequent first order equations.

$$V_1'=-i\alpha U_1,$$
$$U_1''-i\alpha RaP_1-\beta^2U_1=0,$$
$$V_1''-RaP_1'-{\beta_1}^2V_1=0. \quad (4.\ 35)$$

First-order equation has following solutions:

$$V_1(y)=C_6\mathrm{cosh}a_3y\ +C_5\mathrm{sinh}a_3y\ +C_8\mathrm{cosh}a_4y\ +C_7\mathrm{sinh}a_4y\,,$$
$$U_1(y)=C_5b_3\mathrm{cosh}a_3y\ +C_7b_4\mathrm{cosh}a_4y\ +C_6b_3\mathrm{sinh}a_3y\ +C_8b_4\mathrm{sinh}a_4y\,,$$
$$P_1(y)=C_6k_3\mathrm{sinh}a_3y\ +C_5k_3\mathrm{cosh}a_3y\ +C_8k_4\mathrm{sinh}a_4y\ +C_7k_4\mathrm{cosh}a_4y\,. \quad (4.\ 36)$$

Region II

By adding equations (27–30) to equations (4. 24), we get the following first order equations.

$$V_1'=-i\alpha U_1+i\alpha\chi P_1,$$
$$U_1''-\left(\frac{4\alpha^2}{3}+Ra\,(-i\alpha+M)\right)U_1+\frac{i\alpha}{3}V_1'=+i\alpha RaP_1,$$
$$V_1''-\frac{3}{4}\left(\alpha^2-i\alpha Ra\right)V_1-\frac{3}{4}RaP_1'+\frac{i\alpha}{4}U_1'=0. \quad (4.\ 37)$$

First-order equation has following solutions:

$$V_1(y)=C_2\mathrm{cosh}a_1y\ +C_1\mathrm{sinh}a_1y\ +C_4\mathrm{cosh}a_2y\ +C_3\mathrm{sinh}a_2y\,,$$
$$U_1(y)=C_2b_1\mathrm{sinh}a_1y\ +C_1b_1\mathrm{cosh}a_1y\ +C_4b_2\mathrm{sinh}a_2y\ +C_3b_2\mathrm{cosh}a_2y\,,$$
$$P_1(y)=C_2k_1\mathrm{sinh}a_1y\ +C_1k_1\mathrm{cosh}a_1y\ +C_4k_2\mathrm{sinh}a_2y\ +C_3k_2\mathrm{cosh}a_2y\,. \quad (4.\ 38)$$

With the interface and boundary conditions

$$\text{At } y=0, \quad v_1^I = v_1^{II}, \quad u_1^I = u_1^{II}, \quad \tfrac{\mu}{d^*}\left(\left(u_1^I\right)' + i\alpha v_1^I\right) - \left(u_1^{II}\right)' - i\alpha v_1^{II} = 0,$$

$$p_1^I - p_1^{II} = 0\,,$$

$$\text{At } y=-d^*, \quad v_1^I - a\tfrac{i\alpha}{2}e^{\phi} = 0, \quad u_1^I = -k_n\left(u_1^I\right)'.$$

$$At y = 1, \quad v_1^{II} + \frac{i\alpha}{2} = 0, \quad u_1^{II} = k_n\left(u_1^{II}\right)'. \tag{4. 39}$$

Here $\mu = \frac{\mu_I}{\mu_{II}}$.

Equation (4. 25), when combined with Eqs. (4.31-4.33), provide second order equations.

Region I

$$V_{20}' = 0,$$

$$U_{20}'' = kRa - MRaU_{20},$$

Second-order equation has following solutions:

$$V_{20} = D_4,$$

$$U_{20} = D_6\sinh\xi y + D_5\cosh\xi y\ + G\left(y\right). \tag{4. 40}$$

Equation (4. 26), when combined with Equations (4.31-4.34), yields second order equations.

Region II

$$D_{20} = \chi^2 P_1\overline{P_1} + \chi P_{20},$$

$$-P_{20}' + \frac{4}{3Ra}V_{20}'' = F,$$

$$-MRaU_{20} + U_{20}'' = RaL,$$

$$V_{20}' = -\chi E\left(y\right). \tag{4. 41}$$

Second-order equation has following solutions:

$$V_{20} = D_1 - \chi\left(V_1\overline{P_1} + P_1\overline{V_1}\right),$$

$$U_{20} = D_2\cosh\xi y\ + D_3\sinh\xi y\ + H\left(y\right),$$

$$P_{20} = D_4 - \frac{4\chi E\left(y\right)}{3Ra} - \int_{y_1}^{y_2} F\left(r\right)dr. \tag{4. 42}$$

$$\text{At } y=-d^*, \quad u_{20}^I + k_n\left(u_{20}^I\right)' - \tfrac{1}{2}\left(\left(u_1^I\right)' + \overline{\left(u_1^I\right)}' + k_n\left(u_1^I\right)'' + \overline{\left(u_1^I\right)}''\right) = 0,$$

$$\text{At } y=1, \quad u_{20}^{II} + k_n\left(u_{20}^{II}\right)' + \tfrac{1}{2}\left(\left(u_1^{II}\right)' + \overline{\left(u_1^{II}\right)}' + k_n\left(u_1^{II}\right)'' + \overline{\left(u_1^{II}\right)}''\right) = 0.$$

$$\text{At } y=0, \quad u_{20}^{II} + \tfrac{1}{2}\left(\left(u_1^{II}\right)' + \overline{\left(u_1^{II}\right)}'\right) - u_{20}^I - \tfrac{1}{2}\left(\left(u_1^I\right)' + \overline{\left(u_1^I\right)}'\right) = 0,$$

$$\frac{\mu}{d^*}\begin{pmatrix} \left(u_{20}^I\right)' + \tfrac{1}{2}\left(\left(u_1^I\right)'' + \overline{\left(u_1^I\right)}''\right) + \tfrac{i\alpha}{2}\left(\left(v_1^I\right)' - \overline{\left(v_1^I\right)}'\right) - \left(u_{20}^{II}\right)' \\ +\tfrac{1}{2}\left(\left(u_1^{II}\right)'' + \overline{\left(u_1^{II}\right)}''\right) + \tfrac{i\alpha}{2}\left(\left(v_1^{II}\right)' - \overline{\left(v_1^{II}\right)}'\right) \end{pmatrix} = 0. \tag{4. 43}$$

As obtained from [20&21], the mean net axial velocity $< u >$ is shown below:

$$< u >= \epsilon^2\left({U_{20}}^I + {U_{20}}^{II}\right). \tag{4. 44}$$

The following is how the flow rate is defined [12&15]

$$Q^I = \epsilon^2 \int_d^0 {U_{20}}^I dy, \tag{4. 45}$$

$$Q^{II} = \epsilon^2 \int_0^1 {U_{20}}^{II} dy. \tag{4. 46}$$

Each constant used in the aforementioned equations has description in the appendix.

5. Results and discussion

The two-layer peristaltic transport of gas and liquid in an asymmetric channel is investigated in this work. Interfacial boundary conditions are taken into consideration when doing flow analysis. The purpose of this section is to show how the mean axial velocity and flow rate change for significant factors. Red lines indicate the liquid phase, and black lines indicate the gas phase. We considered air as the gas and water as the liquid phase in order to compile the data.

The variation in mean axial velocity for the input parameters are depicted in figures 2-7. Fig 2 illustrates the behavior of mean axial velocity for compressibility parameter χ. It is detected that the velocity decreases with rise in χ in the middle of the channel while reverse behavior is depicted next to the channel walls at both region I and II. The reason is that the compressible fluid responds more strongly to pressure gradients, causing a reduction in velocity. The slip effect might dominate near the walls, leading to increased velocities compared to the interface. Fig. 3 demonstrated the impact of wave number α against velocity profile. It is noticed that the velocity of the fluid decreases at the interface while increases near the walls of the channel. Fig. 4 shows the variation in velocity for slip parameter k_n. The decreasing behavior for velocity is observed for rise in k_n. Fig. 5 represents the variation in mean axial velocity for magnetic parameter M. It is detected that by increasing M the velocity of the flow decreases. Fig. 6 is plotted to observe the velocity variation against phase difference ϕ. It is perceived that by increasing ϕ the velocity of both regions increases at the interface while opposite behavior is depicted near the channel walls. Figure 7 illustrates how increasing Ra increases mean velocity. Ra represents the ratio of viscous to inertial forces. When Ra is increased, the viscous forces decrease. Reduced viscous forces indicate that the fluid is less likely to obstruct flow. As a result, the fluid's velocity will probably rise as a result of the reduced viscous forces. When plotting Fig. 8, air-water and motor oil-air are taken into account. Plotting for various viscosity ratios is shown in Figure 8. It is noted that velocity decreases for increasing μ. This is because higher viscosity fluid experiences greater resistance to flow compared to lower viscosity fluid, resulting in a more significant slowdown in its velocity.

Plotting of the flow rates in both regions against various parameters is shown in Figs. 9–12. Figures 9 and 10 show that as the Reynolds number and magnetic field parameter increase, the flow rate of the compressible flow region decreases. Figures 11 and 12 represents that the *Ra* and *M* lowered the flow rate of second region.

The design of heat exchangers and cooling systems, especially in situations involving two-phase flow (gas-liquid), like nuclear reactors, electronic cooling, or chemical processing, are among the most direct uses of this research. The use of magnetic fields to regulate

simultaneous flows of liquid metals and gasses is already well-established in the metallurgical industry. This work sheds light on the effectiveness of magnetohydrodynamics (MHD) in wavy channels, which could aid in the improvement of processes like metal cooling, smelting, and electromagnetic casting. Higher-quality materials and more energy-efficient procedures may result from the capacity to regulate the behavior of liquid metals under stratified magnetic fields.

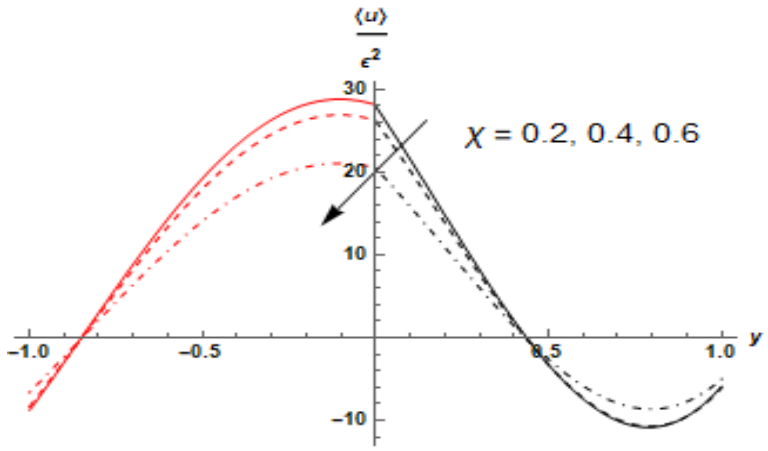

FIGURE 2. Variation in $< u >$ for χ by using $(\mu = 0.02, \alpha = 0.05, M = 0.1)$

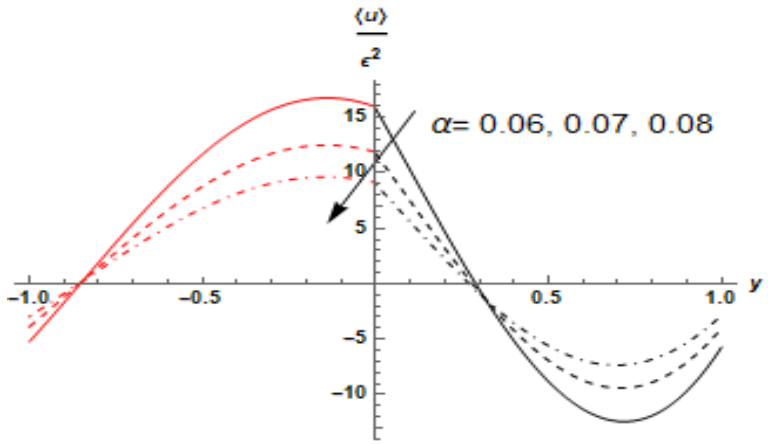

FIGURE 3. Variation in $< u >$ for α by using $(\mu = 0.02, \alpha = .05, M = 0.1)$

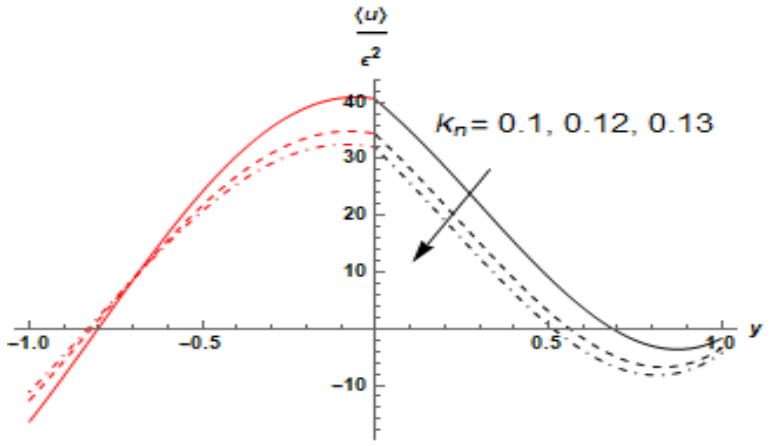

FIGURE 4. Variation in $< u >$ for k_n by using ($\mu = 0.02, \alpha = .05, M = 0.1$)

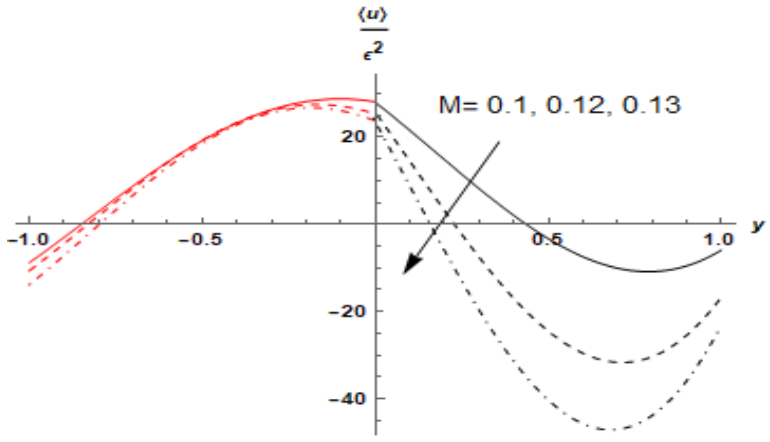

FIGURE 5. Variation in $< u >$ for M by using ($\mu = 0.02, \alpha = .05, Ra = 50$)

6. CONCLUSION

Stratified flow is considered in asymmetric peristaltic channel to advance the understanding of two-phase flow. The hydromagnetic effect is incorporated in both regions. Perturbation technique is used to find the analytic solution of the problem. The expression for axial velocity and flow rate is plotted to examine the behavior of various parameters. This type of flow in not considered yet in peristaltic channel, so the outcomes of the current study would advance the literature and explore new areas of future research. The primary findings of the current research are:

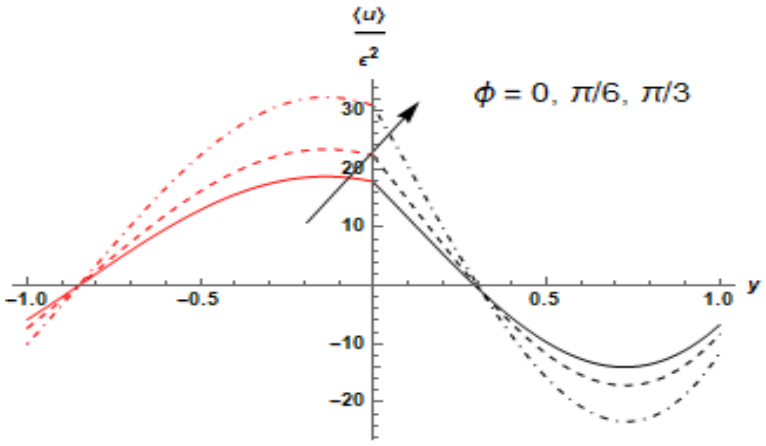

FIGURE 6. Variation in $< u >$ for ϕ by using ($\mu = 0.02, \alpha = .05, M = 0.1$)

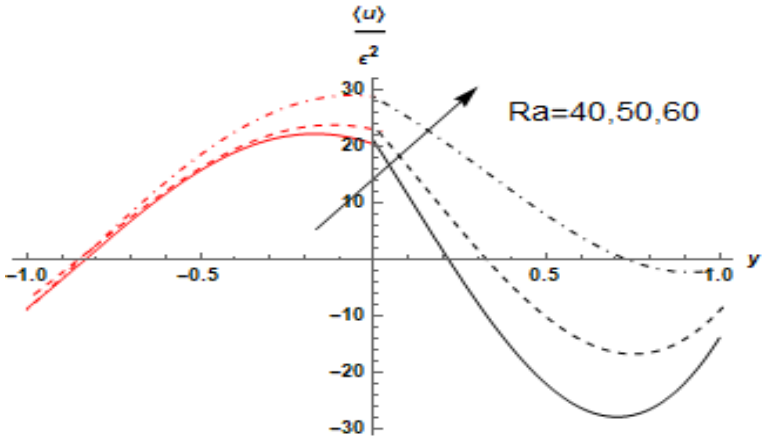

FIGURE 7. Variation in $< u >$ for Ra by using ($\mu = 0.02, \alpha = .05, M = 0.1$)

(1) At the interface, the axial velocity of both sections decreases as the wave number α and compressibility parameter increase, whereas the reverse behavior is seen near to the channel wall.
(2) The magnetic parameter *M* causes the velocity of the flow to decreases.
(3) As Reynolds number *Ra* rises, the mean axial velocity of both sections rises as well.
(4) *Ra* and *M* increases cause the flow rates in both regions to drop.

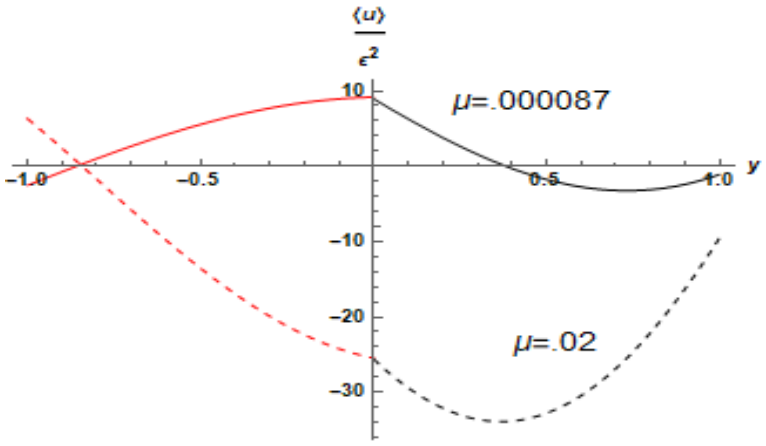

FIGURE 8. Variation in $< u >$ for μ by using ($Ra = 50, \alpha = .05, M = 0.1$)

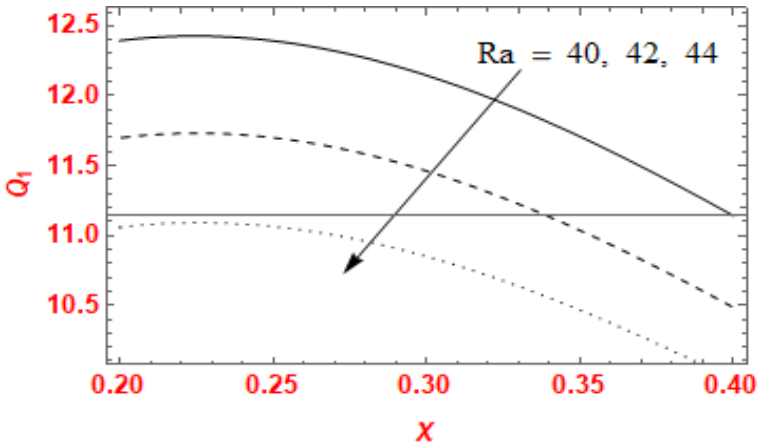

FIGURE 9. Variation in Q_1 for Ra

(5) Motor oil is more viscous than water, therefore viscosity ratio of air-water is higher than air-motor oil. By increasing viscosity ratios, significant decrease in velocity is observed.

Limitations

(1) Surface tension effects at the gas-liquid interface, which might affect the flow, is not incorporated in the current model.
(2) Heat transfer is not included in the model, but in practical applications, temperature gradients play a significant role in altering both the flow and magnetic properties.

Future Directions:

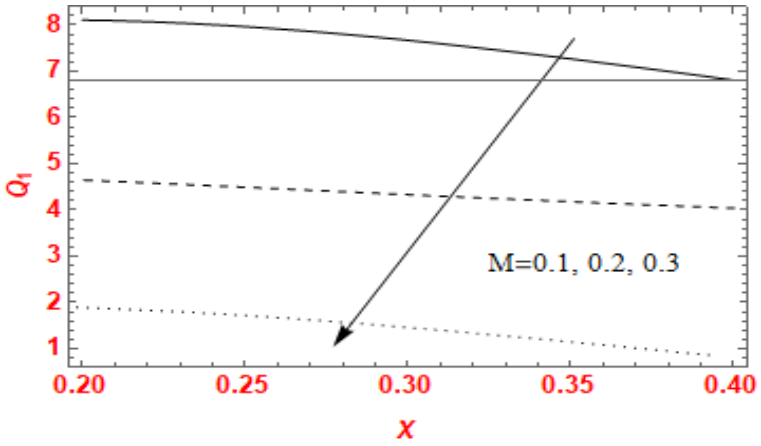

FIGURE 10. Variation in Q_1 for M

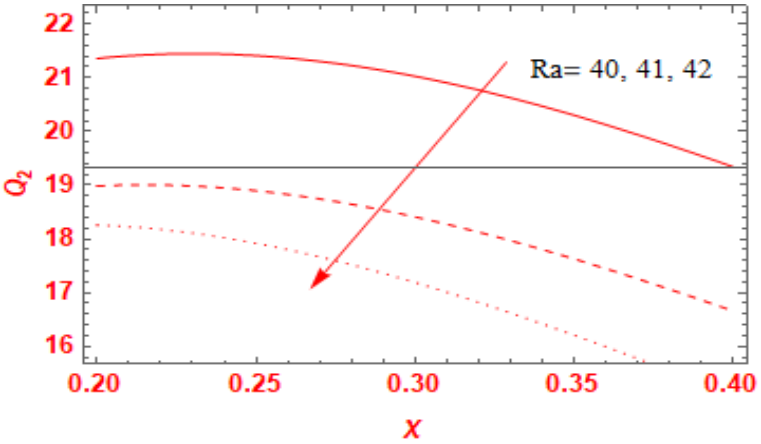

FIGURE 11. Variation in Q_2 for Ra

The approach could be expanded by incorporating variable fluid properties with variable magnetic field in flow patterns. New fields of study would be made possible by investigating the effects of phase changes (such as evaporation or condensation) on stratified hydromagnetic flows in wavy channels, especially for applications like boiling or condensation in nuclear reactors.

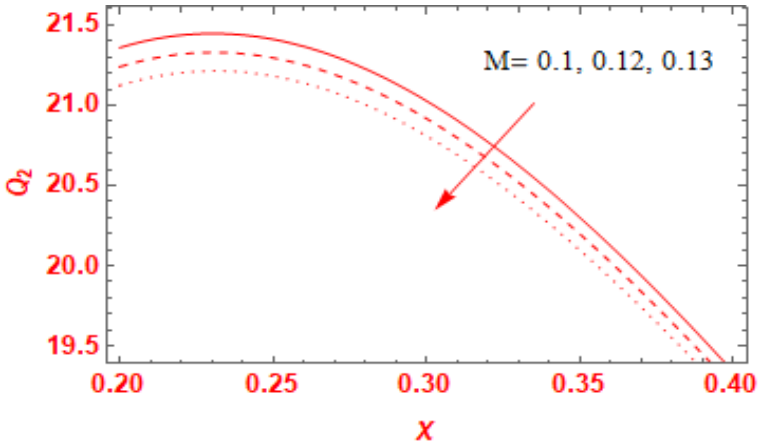

FIGURE 12. Variation in Q_2 for M

Appendix

$$a_1 = \sqrt{\frac{\sqrt{-4{\beta_1}^2{\nu_1}^2 + \left(\beta^2+\nu^2\right)^2} + \left(\beta^2+\nu^2\right)}{2}},$$

$$a_2 = \sqrt{\frac{\left(\beta^2+\nu^2\right) - \sqrt{-4{\beta_1}^2{\nu_1}^2 + \left(\beta^2+\nu^2\right)^2}}{2}},$$

$$a_3 = \sqrt{\frac{\left(\beta^2+\alpha^2\right) + \sqrt{\left(\beta^2+\alpha^2\right)^2 - 4{\beta_1}^2{\alpha_1}^2}}{2}}$$

$$a_4 = \sqrt{\frac{\left(\beta^2+\alpha^2\right) - \sqrt{\left(\beta^2+\alpha^2\right)^2 - 4{\beta_1}^2{\alpha_1}^2}}{2}},$$

$$\nu_1 = \sqrt{\beta^2 - \frac{\left(\beta^2-\alpha^2\right)}{\Gamma}},\ \nu = \sqrt{{\beta_1}^2 - \frac{\left({\beta_1}^2-\alpha^2\right)}{\Gamma}},\quad \Gamma = 1 - \frac{i\chi\alpha}{\gamma}\ ,\ \beta_1 = \sqrt{\alpha^2 - i\alpha Ra},$$

$$\gamma = Ra - \frac{i\chi\alpha}{3},\ \ \beta = \sqrt{\alpha^2 + (M - i\alpha)\,Ra}\ ,\ \ b_1 = \chi\frac{\left(-{\beta_1}^2 + {a_1}^2\right)}{\gamma a_1} + \frac{ia_1}{\alpha},$$

$$b_2 = \chi\frac{\left(-{\beta_1}^2 + {a_2}^2\right)}{\gamma a_2} + \frac{ia_2}{\alpha}, b_3 = \frac{ia_3}{\alpha},\ \ b_4 = \frac{ia_4}{\alpha},$$

$$k_1 = \frac{\left(-{\beta_1}^2 + {a_1}^2\right)}{\gamma a_1},\ k_2 = \frac{\left(-{\beta_1}^2 + {a_2}^2\right)}{\gamma a_2},\ k_3 = \frac{\left(-{\beta_1}^2 + {a_3}^2\right)}{a_3 Ra},$$

$$k_4 = \frac{\left(-{\beta_1}^2 + {a_4}^2\right)}{a_4 Ra},\ \xi = \sqrt{M * \mathrm{Ra}},$$

$$H(y) = Ra \left(\begin{array}{c} \frac{J_1 sinh(a_1+\overline{a_1})y + J_2 cosh(a_1+\overline{a_1})y}{(a_1+\overline{a_1})^2 - \xi^2} + \frac{J_3 sinh(-\overline{a_1}+a_1)y + J_4 cosh(-\overline{a_1}+a_1)y}{(a_1-\overline{a_1})^2 - \xi^2} \\ + \frac{J_5 sinh(a_1+\overline{a_2})y + J_6 cosh(a_1+\overline{a_2})y]}{(a_1+\overline{a_2})^2 - \xi^2} + \frac{J_7 sinh(-\overline{a_2}+a_1)y + J_8 cosh(-\overline{a_2}+a_1)y]}{(a_1-\overline{a_2})^2 - \xi^2} \\ + \frac{J_9 sinh(a_2+\overline{a_1})y + J_{10} cosh(a_2+\overline{a_1})y}{(a_2+\overline{a_1})^2 - \xi^2} + \frac{J_{11} sinh(-\overline{a_1}+a_2)y + J_{12} cosh(-\overline{a_1}+a_2)y}{(a_2-\overline{a_1})^2 - \xi^2} \\ + \frac{J_{13} sinh(a_2+\overline{a_2})y + J_{14} cosh(a_2+\overline{a_2})y}{(a_2+\overline{a_2})^2 - \xi^2} + \frac{J_{15} sinh(-\overline{a_2}+a_2)y + J_{16} cosh(-\overline{a_2}+a_2)y}{(a_2-\overline{a_2})^2 - \xi^2} \end{array} \right),$$

$$G(y) = Ra \left(\begin{array}{c} \frac{l_1 sinh(\overline{a_3}+a_3)y + l_2 cosh(\overline{a_3}+a_3)y}{(a_3+\overline{a_3})^2 - \xi^2} + \frac{l_3 sinh(-\overline{a_3}+a_3)y + l_4 cosh(-\overline{a_3}+a_3)y}{(a_3-\overline{a_3})^2 - \xi^2} \\ + \frac{l_5 sinh(a_3+\overline{a_4})y + l_6 cosh(a_3+\overline{a_4})y]}{(a_3+\overline{a_4})^2 - \xi^2} + \frac{l_7 sinh(-\overline{a_4}+a_3)y + l_8 cosh(-\overline{a_4}+a_3)y]}{(a_3-\overline{a_4})^2 - \xi^2} + \\ \frac{l_9 sinh(a_4+\overline{a_3})y + l_{10} cosh(a_4+\overline{a_3})y}{(a_4+\overline{a_3})^2 - \xi^2} + \frac{l_{11} sinh(a_4-\overline{a_3})y + l_{12} cosh(a_4-\overline{a_3})y}{(a_4-\overline{a_3})^2 - \xi^2} + \\ \frac{l_{13} sinh(a_4+\overline{a_4})y + l_{14} cosh(a_4+\overline{a_4})y}{(a_4+\overline{a_4})^2 - \xi^2} + \frac{l_{15} sinh(a_4-\overline{a_4})y + l_{16} cosh(a_4-\overline{a_4})y}{(a_4-\overline{a_4})^2 - \xi^2} \end{array} \right).$$

References

(1) A. Ali, M. Awais, A. Al-Zubaidi, S. Saleem, and D. K. Marwat. *Hartmann boundary layer in peristaltic flow for viscoelastic fluid: Existence*. Ain Shams Engineering journal **13**, No. 2 (2022): 101555

(2) A. Ali, A. Barman, and S. Das. *Electromagnetic phenomena in cilia actuated peristaltic transport of hybrid nano-blood with Jeffrey model through an artery sustaining regnant magnetic field*. Waves in Random and Complex Media, (2022): 1-32.

(3) A. Ali, S. Sarkar, S. Das, and R. N. Jana. *Investigation of cattaneo–christov double diffusions theory in bioconvective slip flow of radiated magneto-cross-nanomaterial over stretching cylinder/plate with activation energy*. International Journal of Applied and Computational Mathematics **7**, No. 5 (2021): 208.

(4) A. K. Alzahrani, Z. Abbas, and M. Z. Ullah. *chemically reactive two-phase flow of viscous-Casson fluids in a rotating channel*. Alexandria Engineering Journal **62**, (2023): 403-413

(5) D. Canuto, and K. Taira. *Two-dimensional compressible viscous flow around a circular cylinder*. Journal of Fluid Mech **785**, (2015): 349-371.

(6) S. Das, N. Mahato, A. Ali, and R. N. Jana. *Dynamical behaviour of magneto-copper-titania/water-ethylene glycol stream inside a gyrating channel*. Chemical Physics Letters **793**, (2022): 139476.

(7) I. M. Eldesoky, M. S. Nayel, A. A. Galal, and H. M. Raslan. *Impact of compliant wall properties on peristaltic transport of a compressible non-newtonian maxwellian fluid through axisymmetric cylindrical tube*. Journal of Physics **1970**, No. 1 (2021): 012001

(8) T.W. Engelmann. *Zur physiologie des ureter*. Archiv für die Gesamte Physiologie des Menschen und der Tiere **2**, No. 1 (1869): 243-293

(9) Z. K. Gao, M. X. Liu, W. D. Dang, and Q. Cai. *A novel complex network-based deep learning method for characterizing gas–liquid two-phase flow*. Petroleum science **18**, (2021): 259-268

(10) W. Guo, F. Kong, X. He, C. Wang, Y. Liu, L. Tong, and C. Liu. *Distribution law of Taylor bubble/liquid slug length in oil–gas–water slug flow and the measurement of gas/liquid flow rates based on thermal diffusion*.Applied thermal engineering **236** (2024): 121886.

(11) M. A. Hussain, and R. Gupta. *A Navier-slip model for liquid film thickness in gas–liquid slug flow in capillaries*. Indian chemical engineer, (2024): 1-16.
(12) A. Jarauta, V. Zingan, P. Minev, and M. Secanell. *A compressible fluid flow model coupling channel and porous media flows and its application to fuel cell materials*. Transport in Porous Media **134**, No. 2 (2020): 351-386
(13) M. Jawad, K. Shehzad, and R. Safdar. *Novel computational study on MHD flow of nanofluid flow with gyrotactic microorganism due to porous stretching sheet*. Punjab Univ. J. Math. **52**, No.12 (2021): 43-60.
(14) A. A. Khan. *Peristaltic movement of a dusty fluid in a curved configuration with mass transfer*. Punjab Univ. J. Math. **53**, No. 1 (2021): 55-71
(15) E. Kükrer, and N. Eskin. *Air–Water Two-Phase Flow Dynamics Analysis in Complex U-Bend Systems through Numerical Modeling*. Computation **12**, (2024): 81.
(16) T.W. Latham. *Fluid motions in a peristaltic pump (Doctoral dissertation*. Massachusetts Institute of Technology) (1966).
(17) L. B. McCash, S. Nadeem, S. Akhtar, A. Saleem, S. Saleem, and A. Issakhov. *Novel idea about the peristaltic flow of heated Newtonian fluid in elliptic duct having ciliated walls*.Alexandria Engineering Journal **61**, No. 4 (2022): 2697-2707
(18) K. S. Mekheimer, S. R. Komy, and S. I. Abdelsalam. *Simultaneous effects of magnetic field and space porosity on compressible Maxwell fluid transport induced by a surface acoustic wave in a microchannel*. Chinese Physics B **22**, No. 12 (2013): 124702.
(19) Z. Nisar, T. Hayat, A. Alsaedi, and B. Ahmad. *Wall properties and convective conditions in MHD radiative peristalsis flow of Eyring–Powell nanofluid*. Journal of Thermal Analysis and Calorimetry **144**, (2021): 1199-1208
(20) R. Rafaqat, and A. A. Khan. *Effects of magnetic field and porosity on compressible flow in an asymmetric channel*. International journal of modern physics B **38**, No. 19 (2023): 2450246.
(21) R. Rafaqat, and A. A. Khan. *Thermal analysis of an unsteady compressible flow in an asymmetric channel with joule heating: a finite difference approach*. Journal of Thermal Analysis and Calorimetry **148**, No. 24 (2023): 14243-14252
(22) M. Rafiq, A. Shaheen, Y. Trabelsi, S. M. Eldin, M. I. Khan, and D. K. Suker. *Impact of activation energy and variable properties on peristaltic flow through porous wall channel*.Scientific reports **13**, No. 1 (2023): 3219
(23) C. Rajashekhar, G. Manjunatha, K. V. Prasad, B. B. Divya, and H. Vaidya. *Peristaltic transport of two-layered blood flow using Herschel–Bulkley Model*. Cogent engineering **5**, No. 1 (2018): 1495592
(24) N. K. Ranjit, G. C. Shit, and D. Tripathi. *Electrothermal analysis in two-layered couple stress fluid flow in an asymmetric microchannel via peristaltic pumping*. Journal of Thermal Analysis and Calorimetry **144**, No. 4 (2021): 1325-1342
(25) N. K. Ranjit, G. C. Shit, and D. Tripathi. *Entropy generation and Joule heating of two layered electroosmotic flow in the peristaltically induced micro channel*. International journal of mechanical sciences **153**, (2019): 430-444
(26) A. R. Rao, and S. Usha. *Peristaltic transport of two immiscible viscous fluids in a circular tube*. Journal of Fluid Mechanics **298**, (1995): 271-285

(27) M. Rashid, K. Ansar, and S. Nadeem. *Effects of induced magnetic field for peristaltic flow of Williamson fluid in a curved channel*. Physica A: Statistical Mechanics and its Applications, 553 (2020): 123979

(28) M. A. Sadiq Murad, and F. K. Hamasalh. *Numerical study for fractional-order magnetohydrodynamic boundary layer fluid flow over stretching sheet*. Punjab Univ. J. Math. **55**, No. 2 (2023): 71-87.

(29) A. H. Shapiro, M. Y. Jaffrin, and S. L. Weinberg. *Peristaltic pumping with long wavelengths at low Reynolds number*. Journal of Fluid Mech **37**, No. 4 (1969): 799-825

(30) J. B. Shukla, R. S. Parihar, B. R. P. Rao, and S. P. Gupta. *Effects of peripheral-layer viscosity on peristaltic transport of a bio-fluid*. Journal of Fluid Mechanics **97**, No. 2 (1980): 225-237.

(31) V. P. Srivastava, and M. Saxena. *A two-fluid model of non-Newtonian blood flow induced by peristaltic waves*.Rheologica acta **34**, (1995): 406-414

(32) A. Tanveer, M. B. Ashraf, and M. Masood. *Entropy analysis of peristaltic flow over curved channel under the impact of MHD and convective conditions*. Numerical Heat Transfer, Part B: Fundamentals **85**, No. 1 (2024): 45-57

(33) Z. Wang, K. Chen, S. Pan, P. Ji, J. Zhang, X. Sun, and B. Sun. *Experimental research on the transformation of gas-oil two-phase flow pattern in large vertical annulus*. Geoenergy Science and Engineering, (2024): 213035.

(34) J. Wu, L. Liu, and T. Liu. *Fundamental theories of aerodynamic force in viscous and compressible complex flows*. Progress in Aerospace Sciences **99**, (2018): 27-63

(35) Y. Zhang, C. He, and P. Li. *Numerical investigation of gas-liquid two-phase flow in horizontal pipe with orifice plate*.Progress in Nuclear Energy **138**, (2021): 103801